Renewable Energy 193 (2022) 870–878

Contents lists available at ScienceDirect

Renewable Energy

journal homepage: www.elsevier.com/locate/renene

Experimental performance of a novel scraped surface heat exchanger for latent energy storage for domestic hot water generation

A. Egea*, A. García, R. Herrero-Martín, J. Pérez-García

Department of Thermal and Fluid Engineering, Polytechnic University of Cartagena, Cartagena, Spain

ARTICLE INFO

Article history:
Received 7 December 2021
Received in revised form
8 March 2022
Accepted 9 May 2022
Available online 16 May 2022

Keywords:
Phase change material
Scraped surface heat exchanger
Solidification
Solar latent thermal energy storage
Domestic hot water

ABSTRACT

In this work, a novel design of a real scale Scraped Surface Heat Exchanger (SSHE) for solar LTES has been developed and experimentally tested. The main issue in PCM heat exchangers is the growth of a solid layer at the heat transfer walls during the latent energy extraction/discharging, that lowers heat transfer. The removal of the solidified PCM through scraping increases the heat transfer rate with nearly constant heat flux. Those characteristics make it suitable for domestic hot water generation. Discharging tests have been performed in scraping and no scraping modes (SM and nSM). The heat release rate in SM has shown to be between two and three times higher than in nSM. Moreover, in SM there is a complete extraction of the available latent energy (11.9 MJ) in a short period, compared to nSM. Additionally, a performance comparison between the developed SSHE and those available in open literature has been done. The results of heat release density (4 kW/m^2) and overall heat transfer coefficient (1000 W/m^{2}K) have shown similar values, though the scraping mechanism, the rotational speed, the size and their energy capacity are different. The developed design is an appropriate technology to increase the efficiency in solar LTES.

1. Introduction

The use of renewable energies for reducing carbon emissions is experiencing important support in recent years. The programme Horizon Europe [1] promotes an important increase in the use of renewables for energy generation during the period 2021–2027, to reduce fossil fuel consumption [2]. With respect to global thermal energy production, they are expected to account for 14% of the total by 2030, according to the International Energy Agency's (IEA) World Energy Outlook 2021 [3].

Solar energy is a common source of thermal energy production. In this field, the use of Phase Change Materials (PCM) allows solving the time delay between energy consumption and production. Thus, the so-called Latent Thermal Energy Storage (LTES) systems are of great interest in applications such as domestic hot water generation. Those systems use the phase change enthalpy of the PCM alternatively for energy storage (melting) and energy release (solidification). In addition, the PCM can exchange sensible heat, which results in a higher storage density with respect to conventional systems.

Sharma et al. [4] developed new materials suitable for domestic hot water production. Mazman et al. [5] successfully enhanced a conventional solar domestic hot water tank by adding PCM at its top. In the recent work by Abdelsalam et al. [6], they studied numerically the effect of incorporating PCM into the core of a conventional water tank integrated into solar domestic hot water system.

Nevertheless, the integration of LTES systems in solar thermal facilities still lacks some technological solutions that prevent their technical and economic feasibility [7]. Namely, the reduction of the thermal resistance between the PCM and the heat transfer fluid (HTF) during both melting and solidification stages is yet an open question.

Fig. 1 shows a scheme of the temperature profile at both sides of the heat transfer wall. There are four thermal resistances involved in the heat release from liquid PCM to HTF (liquid PCM boundary layer, solid PCM layer, heat transfer wall and HTF boundary layer). The PCM layer growths over time. Because those materials typically present low values of thermal conductivity, the heat transfer

* Corresponding author.
E-mail addresses: alberto.egea@upct.es (A. Egea), alberto.garcia@upct.es (A. García), ruth.herrero@upct.es (R. Herrero-Martín), pepe.perez@upct.es (J. Pérez-García).

https://doi.org/10.1016/j.renene.2022.05.057

Nomenclature

A	Heat transfer surface (m^2)
c_p	Specific heat (kJ/kg·K)
E	Energy (J)
e	Thickness (m)
m	PCM mass
$\dot{m}$	Mass flow rate (kg/s)
$\dot{Q}$	Heat release rate (W)
$\dot{Q}/A$	Heat release density (W/m^2)
T	Temperature (K)
t	Time (s)
U	Overall heat transfer coefficient (W/m^2K)

Greek symbols

β	Solid fraction
ΔE	Energy difference (J)
ΔT	Temperature difference (K)
λ	Enthalpy (J/kg)

Abbreviations

HTF	Heat transfer fluid
LTES	Latent Thermal Energy Storage
nSM	No-Scraping Mode
PCM	Phase Change Material
SSHE	Scraped surface heat exchanger
SM	Scraping Mode

Subscript

in	inlet
l	Latent heat
losses	thermal losses
out	outlet
s	Sensible heat
steel	Heat exchanger steel structure

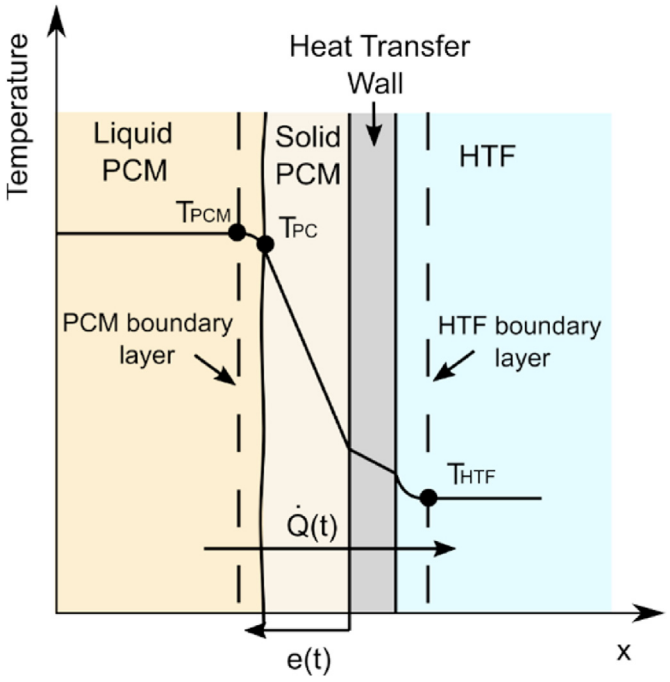

Fig. 1. Temperature profile during PCM solidification.

resistance at the solid layer of PCM becomes dominant at low thicknesses. For a typical heat transfer problem of LTES, the solidified PCM layer clearly dominates the heat transfer resistance if it is thicker than 1 mm [8].

Since conduction is the dominant heat transfer mechanism during solidification, discharging times in PCM heat exchangers are much longer than charging times [9]. To overcome this issue, many authors have studied the effect of conventional passive heat transfer enhancement techniques, such as the use of extended heat transfer surfaces or the addition of high conductive materials/particles to increase the thermal conductivity of the PCM. Ibrahim et al. [10] and later Al-Maghalseh and Mahkamov [11] carried out extensive reviews about the topic. Stritih [12] and Rahimi et al. [13] found that the extraction of heat could be effectively enhanced by adding fins to a given latent-heat storage unit.

On the other side, the European Association for Storage of Energy (EASE) and the European Energy Research Alliance (EERA) have recently identified, among the gaps in research in LTES systems, their inability to separate capacity and power, owing to the passive heat exchange technologies employed up to date [14]. Their roadmap towards 2030 on energy storage claims that research and development on active heat exchangers with controllable heat transfer power need to be undertaken in order to overcome this limitation.

Several concepts of active heat exchangers have been developed: Tay et al. [15] and Gasia et al. [16] recirculated the PCM during the melting process, which resulted in faster melting times. Zhang and Niu [17] designed a microencapsulated PCM slurry thermal storage device with a stirrer; their concept was further enhanced by Delgado et al. [18] who reported an increase in the overall heat transfer coefficient due to the agitation.

Zipf et al. [19] applied the concept of Screw Heat Exchanger (SHE) for active latent heat storage to avoid the growth of solid PCM layer. Pointner and Steinmann [20] developed a novel active latent heat storage concept called PCM flux. They were capable of maintaining a constant and controllable discharging heat flux through the mechanical separation of the storage material from the heat exchanger.

The Scraped Surfaces Heat Exchanger (SSHE) is a promising technology for LTES systems. They provide a high heat transfer rate with nearly constant heat flux and a great increase in flow-mixing. It has been successfully used for ice slurry production [21–23] and food-processing [24], where considerable enhancements have been reported However, there are very few studies on its suitability for PCM applications.

Nepustil et al. [25] designed a novel plate heat exchanger for PCM where the heat transfer surface was scraped by linear action, in order to keep the solid layer of PCM to a constant thickness. They obtained a nearly constant heat flux during the discharging process.

Maruoka et al. [26] developed a SSHE heat exchanger where the rotation of a cylindrical tube against a fixed blade removed the solid layer of PCM during the discharging process. They tested a range of rotational speed 0–500 rpm, and found up to six times increase in the heat release rate compared to the no rotation mode. The solidification was accelerated in the rotation mode, up to 80% of the available latent heat was released in a short period (15 min). In contrast, the system with no scraping was only capable of

extracting 50% of total latent heat after 4 h. They reported a maximum overall heat transfer coefficient of 2000 W/m^{2}K.

In a recent work, Tombrinck et al. [8] experimentally studied a rotating drum heat exchanger for LTES where the heat transfer walls were continuously scraped in order to minimize the layer thickness of the solidified PCM and maximize heat transfer. The range of rotational speed was 0–25 rpm. In that way, the authors were able to control the thermal power output. The heat transfer rate was constant for a given rotational speed and increased with velocity. The scrapping of the solid PCM layer promoted an increase of heat transfer density, with maximum values of 6.8 kW/m^2. Although their prototype was tested with a low melting point fatty acid (decanoic acid), a new experimental test rig for high-temperature applications is being developed. Their future experimental research will be supported by their numerical model [27].

In the present work, a novel real scale scraper rotative heat exchanger is presented for the first time. The prototype is intended to be integrated in solar latent energy thermal storage for domestic hot water production. It has been designed to combine a high capacity of energy storage with a fast controlled response to user energy demand. The selected PCM is an organic paraffin wax that meets the requirements for this application, as several studies have pointed out [28,29]: it is non-toxic and non-corrosive, relatively economical and presents small changes in volume during phase transition.

Experimental tests have been conducted to estimate the enhancement of Scraping Mode over the no-Scraping Mode. First, the visualization of the solidification for both modes has been performed. It allows for a qualitative interpretation of the reported results of heat release rate, HTF temperature increase, solid fraction evolution and overall heat transfer coefficient. A range of rotational speed 0–7.5 rpm has been studied. The results obtained have been compared with those from Maruoka et al. [26] and Tombrink et al. [8], in terms of overall heat coefficient and heat release rate density. The experimental results confirm the great potential of the developed SSHE in latent thermal solar energy storage systems for domestic hot water production.

2. Materials and methods

In this section the developed SSHE, the experimental facility and the PCM properties are presented. Furthermore, the test methodology and the data processing with its uncertainty analysis are described.

2.1. Experimental setup

The SSHE prototype follows a concentric tube heat exchanger design, where the PCM is placed in the inner cylinder and a HTF flows through the outer cylinder (or jacket). A sketch of the active scraper prototype is shown in Fig. 2.

Delving deeper into the design of the prototype, it is made of 316L stainless steel with an outer diameter of 0.4 m, a diameter of the PCM chamber of 0.3 m, and a total height of 1 m. The total volume available for PCM is 0.0675 m^3, which results in a scraped surface to PCM volume ratio of 15 m^2/m^3.

At the top of the exchanger there is a window to visualize its inside. The chamber has three pairs of blades made of POM-C (Polyacetal (Copolymer)). During solidification, they are continuously rotating and removing the solid PCM layer from the inner side of the heat transfer surface. The rotation is produced by an electrical motor and a gear reducer. A frequency converter allows controlling the rotation speed in a range of 3–7.5 rpm. Due to practical limitations, lower velocities cannot be achieved.

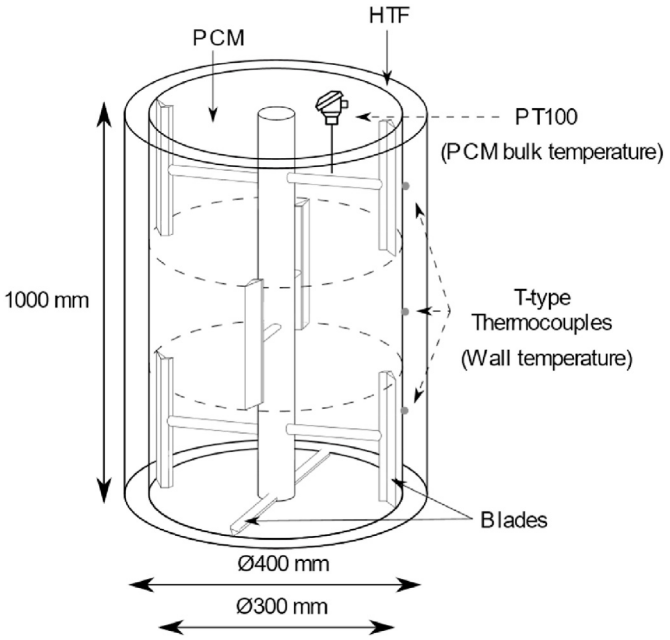

Fig. 2. Sketch of the scraper rotative LTES system.

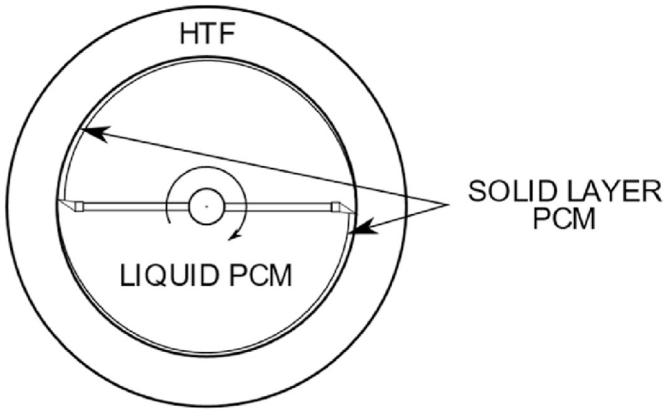

Fig. 3. The basic concept of a section of the scraper rotative LTES system.

Fig. 3 shows how the scraper rotative heat exchanger works. Once the PCM is melted, the flow of HTF at the outer jacket starts to extract energy. As a result, PCM starts to solidify at the inner part of the heat transfer surface. Thanks to the scraping of the wall, blades are constantly removing the solid PCM and thus there is no growth of the thermal resistance layer. In the absence of scraping, the solid layer thickness would gradually be increased, resulting in a rise of thermal resistance and a drastically reduction of the energy extracted.

Fig. 4 shows a sketch and a picture of the experimental facility. Before performing a solidification test, the PCM is preheated to 52 °C to ensure its complete melting. To this aim, there is a set of electric heaters placed at the bottom of the prototype which are controlled by solid-state relays. Once all PCM is melted and the HTF fixed to the test temperature, a variable-speed circulating pump drives the HTF from a tank to the SSHE in a closed circuit.

All the tests are carried out with water as HTF, and the mass flow is fixed to 0.1111 kg/s. Two RTD sensors measure the inlet and the outlet water temperature. During the test the water enters at the

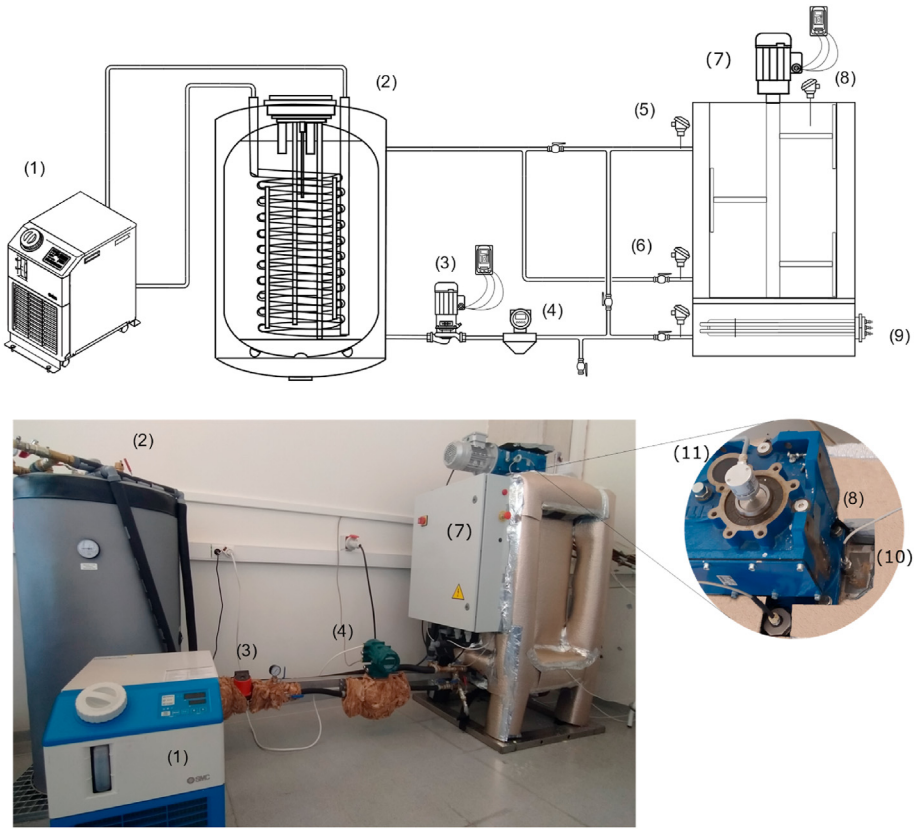

Fig. 4. Experimental setup. (1) Chiller; (2) Heat transfer fluid tank; (3) Pump; (4) Coriolis Flowmeter; (5,6) Inlet/outlet HTF temperature sensors; (7) Scraper rotative LHT storage system; (8) PCM bulk temperature sensor; (9) electrical heater; (10) Visualization window; (11) Digital encoder.

top of the scraper rotative heat exchanger and the inlet HTF temperature is settled to 25 °C. The mass flow rate is obtained by a Coriolis Flowmeter ROTAMASS PRIME 25.

To study the effectiveness of scraping during PCM solidification two different modes have been tested, no-Scraping Mode (nSM) test and Scraping Mode (SM) test with rotational speeds of 3, 5 and 7.5 rpm. A digital encoder measures the rotational speed. The system power consumption during the process has been measured by a power analyzer. A mean value of 200 W for every discharging test was obtained, regardless of the rotational speed. A maximum deviation of 5% was observed from the onset to the end of the solidification process.

The wall temperature of the prototype is measured by several T-type thermocouples placed at the external wall of the PCM chamber. They are fixed at different heights in order to study the stratification of PCM. The thermocouples were previously calibrated in a thermostatic bath and the uncertainty was improved to 0.1 K. The PCM bulk temperature is measured by an RTD sensor placed in the middle of the wall-axe distance. All RTDs in the test rig are PT100 Class B 1/10 DIN sensors.

A chiller (HRS050-AF-20 from SMC) allows setting the water temperature before the test. All the devices used for the system control such as the electric heaters, the chiller, and the frequency converter are controlled by a computer with RS485 communication and a LabVIEW application. Measurements are collected by a data logger (Keysight 34980A).

Finally, in order to estimate the prototype thermal losses to the ambient, controlled constant power is supplied to the electric heaters until the thermal equilibrium of the system is reached and the outer side of the isolation remains at a constant temperature over time. This temperature is measured by T-type thermocouples placed in several positions. The ambient temperature is also measured. In this work, the thermal losses are lower than 5% of the stored energy for all cases of study. Additionally, T-type thermocouples are placed along the steel structure of the exchanger to calculate the sensible energy stored in the steel assembly.

2.2. PCM properties

The PCM used in this work is the commercial paraffin wax RT44HC from Rubitherm GmbH [30]. For practical purposes, it has a melting point slightly below what is needed for domestic hot water production. Their properties are listed in Table 1, as given by the supplier. Additionally, PCM properties were measured with Differential Scanning Calorimetry (DSC). The melting and solidification enthalpies and temperatures were studied and presented in Table 2. The results were close to those reported by the manufacturer, though some differences were found in the melting and solidification ranges. Both ranges were found higher, 41–47 °C and 43–37 °C, respectively.

The measurements for melting and solidification enthalpies were 258 kJ/kg and 253 kJ/kg, respectively. The variations with respect to the values given by Table 1 are probably due to the definition given by the manufacturer (the value of 250 kJ/kg is a combination between latent heat and sensible heat in a range 35–50 °C). In Table 2 the differences are presented.

2.3. Data reduction

2.3.1. Heat release

The heat release rate to the water for every time step is computed as:

Table 1
Physical properties of RT44HC as given by Rubitherm GmbH.

Melting Area	41–44	[°C]
Solidification Area	44–40	[°C]
Heat storage capacity ± 7.5%, (Temperature range = 35 °C to 50 °C)	250	[kJ/kg]
Specific heat capacity	2	[kJ/kg·K]
Density solid (T = 25 °C)	0.8	[kg/L]
Density liquid (T = 80 °C)	0.7	[kg/L]
Heat conductivity	0.2	[W/m·K]
Volume expansion	12.5	[%]
Max. operation temperature	70	[°C]

Table 2
Rt44HC measured melting and solidification parameters.

Property	Manufacturer	Measured
Melting area [°C]	41–44	41–47
Solidification area [°C]	44–40	43–37
Melting enthalpy [kJ/kg]	250	253
Solidification enthalpy [kJ/kg]	250	258

$$\dot{Q}(t) = \dot{m}\, c_p\, (T_{out} - T_{in}) \tag{1}$$

where T_{out} and T_{in} are the outlet and inlet water temperatures, $\dot{m}$ is the water mass flow rate and c_p is the water-specific heat.

2.3.2. Energy release

It is possible to calculate the amount of released energy to the water by integrating the heat release rate for a given period, following eq. 2

$$E = \int_{t_1}^{t_2} \dot{Q}(t)\, dt. \tag{2}$$

2.3.3. Solid fraction

The solid fraction evolution in SM is calculated from the release of PCM latent energy according to eq. (3). It refers to the ratio of solidified PCM to the total amount of PCM in the system:

$$\beta_{SM} = \frac{E_{PCM,l}}{\lambda} \tag{3}$$

where λ refers to the total PCM phase change enthalpy (Table 1) and $E_{PCM,l}$ is calculated from the energy balance given by eq. (4) for every time step.

$$E_{PCM,l} = (E - E_{PCM,s}) + E_{losses} - E_{steel} \tag{4}$$

where E_{losses} accounts for the thermal ambient losses, E_{steel} is the released energy by the steel of the heat exchanger to the water flow and $E_{PCM,s}$ is the initial release of sensible energy before the solidification starts:

$$E_{PCM,s} = m\, c_p\, (\Delta T) \tag{5}$$

where m and c_p are the mass and the specific heat of PCM, respectively (Table 1).

In the nSM, the contribution of the solidified PCM sensible heat to the total heat release cannot be determined, because the thickness of the solid PCM layer is unknown. For this reason, the solid fraction evolution in the nSM has been estimated from direct measurements of the solid layer thickness through the visualization window. The solid fraction in this mode has been calculated as:

$$\beta_{nSM} = \frac{Volume\ of\ solidified\ PCM}{Volume\ of\ PCM} \tag{6}$$

2.3.4. Overall heat transfer coefficient

Similarly to Maruoka et al. [26], it has been assumed a countercurrent heat exchanger performance for the SSHE described in this work. Therefore, the overall heat transfer coefficient, U, can be estimated as:

$$U = \frac{\dot{Q}}{A\, \frac{\Delta T1 - \Delta T2}{\ln(\Delta T1/\Delta T2)}} \tag{7}$$

where A is the heat transfer surface and $\Delta T1$ and $\Delta T2$ are defined in eq. (8) and eq. (9) respectively:

$$\Delta T1 = T_{PCM} - T_{out} \tag{8}$$

$$\Delta T2 = T_{PCM} - T_{in} \tag{9}$$

where T_{PCM} is the PCM bulk temperature.

2.4. Uncertainty analysis

Experimental uncertainty was calculated following the Kline and McClintock [31] method based on a 95% confidence level. Instrumentation errors were as follows: temperature, 0.03 °C; flow rate, 0.1% measure. The uncertainty for c_p was estimated according to the estimated error in the temperature measurement and was found to be negligible. An uncertainty of 0.1% was allocated to both the inner diameter and height of the SSHE. Uncertainty calculations showed maximum values of 1.7% for heat transfer rate ($\dot{Q}$) and heat transfer density ($\dot{Q}/A$) and 1.9% for overall heat transfer coefficient (U). As those values are very low, no error bars are given in the experimental results figures.

3. Results and discussion

In this section, the main results of this study are presented. The visualization of the solidification process, the heat release rate results, the wall temperature evolution over time, the solid fraction and the overall heat transfer coefficient allow to a better assessment of the SSHE performance.

3.1. Visualization of the solidification process

The observation of the phase change process over time helps for a better interpretation of the experimental results. The window placed at the top of the prototype (Fig. 4) allows obtaining pictures of the solidification of PCM. Fig. 5 shows three images taken at t = 0.4 h (Time I), t = 0.8 h (Time II) y t = 1.2 h (Time III), for the nSM (left) and the SM (right) at rotational speed of 5 rpm.

The values of the Times I and III have been selected according to the moment when the T_{PCM} reaches its phase change value for each mode. T = 43 °C has been considered as representative of the beginning of solidification (Table 2). Fig. 6 shows the evolution of T_{PCM} over time; the solidification onset takes place 3 times later SM (Time (I), 0.4 h) than in nSM (Time (III), 1.2 h).

As shown in Fig. 5, there is a very different solidification behaviour for both modes. In nSM, there is a continuous growing of

a solid PCM layer adhered to the wall, which increases its thickness from the Time I to III.

However, in SM, at the Time I, it is observed how the action of the scraper removes the solid PCM from the wall. This is incorporated into the core and replaced with liquid which solidifies again. Once there is a significant amount of solidified material (Time II), the remaining liquid PCM gets confined in the solid phase and cannot reach the wall. In addition, the increase of paraffin density after solidification results in a volume reduction that creates a small air gap between PCM and the inner wall jacket chamber. At the Time III all the PCM has reached its solid-state and the small air gap at the wall remains.

3.2. Heat release rate

The heat release rate $\dot{Q}$ results (eq. (1)) along time are presented in Fig. 7, for the no scraping mode (0 rpm) and three different rotation speeds (3, 5 and 7.5 rpm). Additionally, in order to compare with other heat exchanger technologies, the heat transfer rate density related to the heat transfer surface is given in the right axis.

In the nSM, a continuous decrease in the heat release rate is observed, since the growth of the solid PCM layer at the heat transfer wall triggers a dominant thermal resistance [8,9,12]. However, a different trend is observed in the SM. There is an initial decrease due to the release of sensible heat from liquid PCM. Later on, $\dot{Q}$ is maintained nearly constant during approximately 30 min (between 0.25 h and 0.75 h).

A similar behaviour was observed by other authors such as [20,26]. This indicates that heat transfer in this period is dominated by the phase change at the wall. After that, the availability of liquid PCM at the wall diminishes (Fig. 5, SM-Time II), which results in a decrease of the heat release.

The rotational speed has not shown a significant impact on the heat release rate. Similarly, the rest of the variables have shown similar results for the scraping mode at different rotational speeds. This indicates that in all cases the solid layer is kept to a minimum level, thus minimizing its thermal resistance. Hence in the following sections, only the results at 5 rpm will be shown. They are considered to be representative of the scraping mode in the range of study.

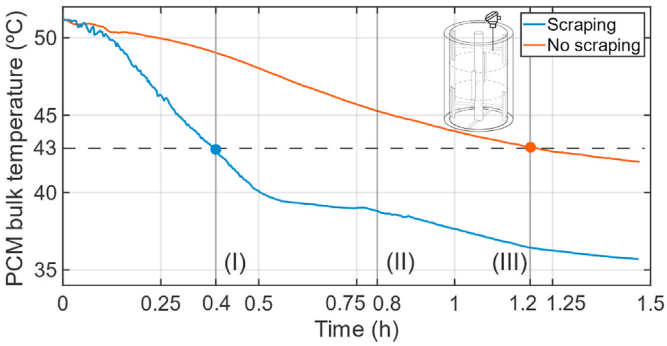

Fig. 6. Evolution of PCM temperature in SM and nSM.

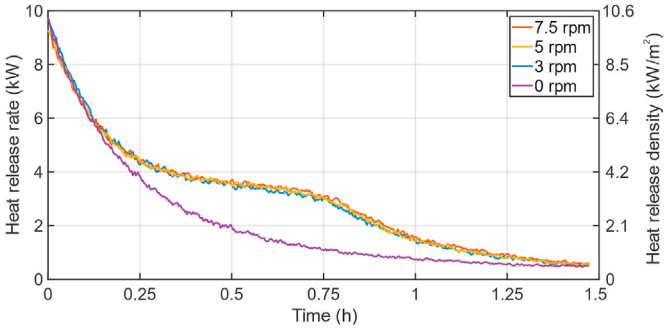

Fig. 7. Heat release rate (left) and heat release rate density (right) over time for different scraping velocities.

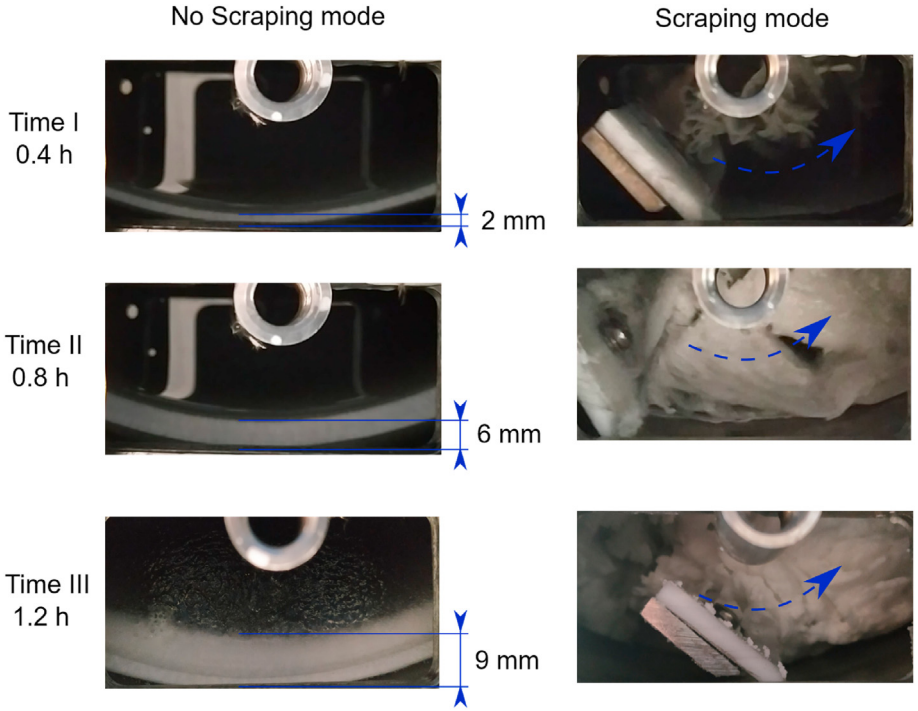

Fig. 5. Pictures of the PCM inside heat exchanger in nSM (left) and SM (right) at Times (I), (II) and (II).

Table 3
Heat release density during solidification.

	Current study (5 rpm)	Tombrink et al. [8] (5 rpm)	Maruoka et al. [26] (100 rpm)
Q̇/A (kW/m2)	4	3.5	4.5

The mean values of heat transfer rate density during the solidification process are compared with those from Maruoka et al. [26] and Tombrink et al. [8], who studied other prototypes of SSHE for LTES. The results are given in Table 3.

To the author's knowledge, this work deals for the first time with a real scale SSHE LTES systems. However, in Refs. [8,26], the researchers studied proofs of concept at a reduced scale. The heat transfer density values obtained at present work are of the same magnitude. The heat release density reported in this work is 10% lower than the one obtained by Maruoka et al. [26], for 20 times less rotational speed.

3.2.1. HTF temperature rise

In domestic hot water systems, there is a need not only for a high energy storage capacity, but for a fast response and a controlled heat release when the users demand the energy. The results shown in previous paragraphs have shown a superior performance in SM over the nSM in terms of heat release. This has a direct impact on the HTF heating, as it is shown in Fig. 8, where the time evolution of the HTF temperature rise, ΔT, is presented for both modes. For the period from 0.25 h to 0.75 h, the values of ΔT in the SM are always higher than in the nSM and present less variations over time (25% vs. 65%).

3.3. Wall temperature

In Fig. 9, the wall temperature evolution at three locations (top, medium, bottom) is presented for the no scraping mode. A continuous decrease is observed in all cases, due to the fact that as the solid layer grows, the phase change is being produced further and further from the wall. Besides, the wall temperature increases from bottom to top. Since cold HTF enters at the upper side of the exchanger, it can be inferred that stratification of the liquid PCM in the inner core of the heat exchanger exists.

On the other hand, it is observed how the stratification still exists in the scraping mode (Fig. 10) but to a lesser extent due to the mixing produced by the rotation. In addition, the wall temperature remains constant over most part of the test (0.25 h–0.75 h). This indicates that the solid PCM layer is being constantly removed and the wall temperature is kept at the phase change temperature.

As the solidification progresses, the scraped solid PCM is displaced from the wall to the inner liquid phase. Because of its higher density with respect to the liquid phase, it sinks to the bottom of the exchanger. Once the solid PCM has reached a given height, the thermal exchange is produced by sensible heat. As a consequence, a temperature decrease in the lower sensor (blue) is observed earlier than in the other positions (0.6 h vs. 0.8 h).

3.4. Solid fraction

The time evolution of PCM solid fraction has been obtained for both the nSM and SM at 5 rpm, according to the procedure described in the data reduction section. The results are shown in Fig. 11 and confirm the experimental trends shown previously.

In the SM, solidification starts around 0.25 h according to the change in the slope of the wall temperature Fig. 10 and heat release rate Fig. 7 curves. The solidification process takes place approximately 1 h after the beginning of the experiment. At this time, the PCM bulk temperature is below 37 °C (Fig. 6), beyond the solidification area given in Table 2. At this moment, the scraping surface heat exchanger has been able to extract 100% of latent energy (11.9 MJ) whereas for the same period with the no scraping mode only a 10% of PCM has already solidified.

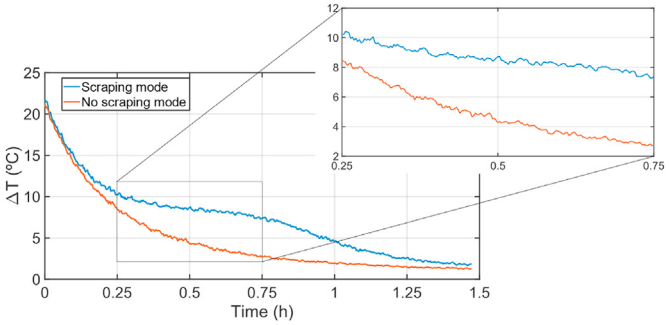

Fig. 8. Time evolution for the temperature difference between outlet and inlet in both modes.

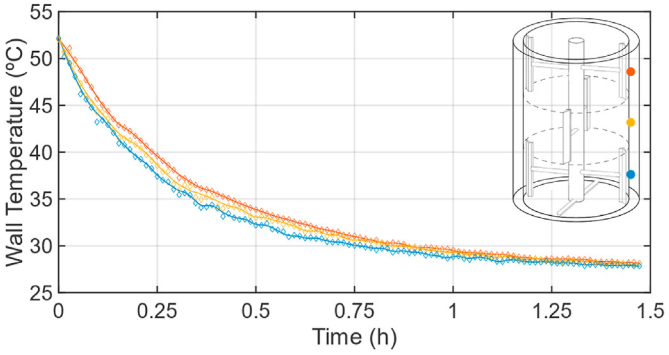

Fig. 9. Wall temperature evolution along time in nSM for three positions: Top (red), medium (yellow) and bottom (blue).

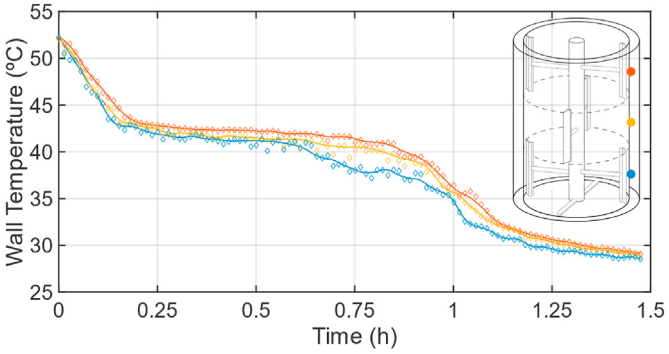

Fig. 10. Wall temperature evolution along time in SM for three positions: Top (red), medium (yellow) and bottom (blue).

3.5. Overall heat transfer coefficient

Fig. 12 shows the overall heat transfer coefficient, *U*, over time in SM and nSM. They are directly linked to the heat release rate (Fig. 7). At 0.75 h the value of *U* in SM is four times higher than in nSM (257 W/m^{2}K vs 60 W/m^{2}K).

In order to compare the performance of the SSHE of this work with that of Maruoka et al. [26], the results of the overall heat

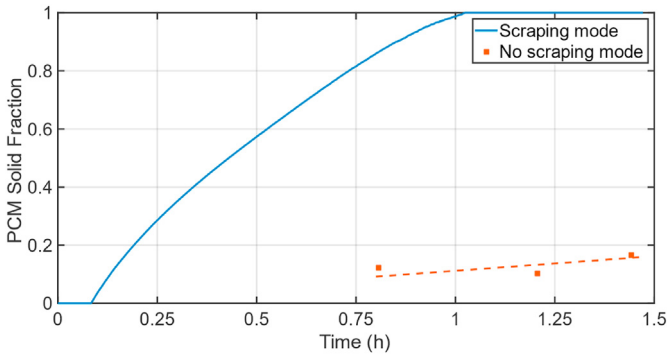

Fig. 11. Solid fraction evolution in scraping mode.

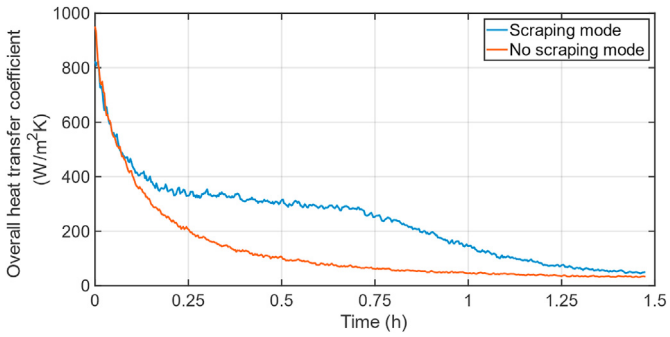

Fig. 12. Overall heat transfer coefficient over time in SM and nSM.

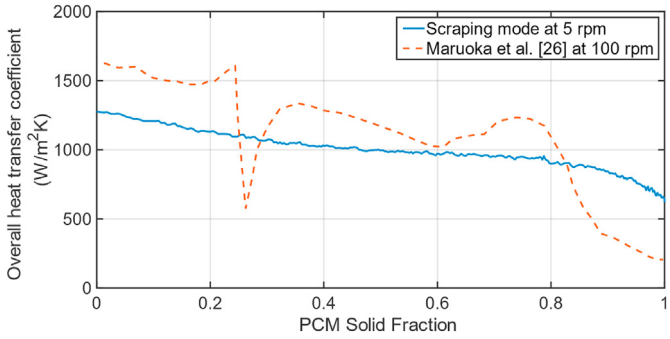

Fig. 13. Overall heat transfer coefficient over PCM solid fraction comparison.

transfer coefficient (based on the total heat transfer surface) are presented as a function of solid fraction in Fig. 13. Despite the fact that in both works the scraping mechanism, the size of the prototype and their energy capacity are different, both studies have reached similar values of U.

The abrupt decrease observed by Maruoka et al. [26] at a solid fraction around 0.25 is due to the type of PCM used (salt hydrate) which presents a supercooling phenomenon. Their average overall heat transfer coefficient is 10% higher than the reported in this study. This is due to the fact that their high level of rotational speed increases the convective heat transfer in the PCM side.

4. Conclusions

In this work, a novel design of a real scale Scraped Surface Heat Exchanger (SSHE) for solar LTES has been tested. It is intended for domestic hot water generation. The PCM is a medium melting temperature commercial paraffin wax. Discharging tests with an outer HTF flow at fixed temperature have been performed in scraping and no scraping modes (SM and nSM). Experimental results have been presented as the evolution over time of heat release rate, heat release density, HTF temperature rise, wall temperature, solid fraction and overall heat transfer coefficient. Additionally, the visualization of the phase change process over time has allowed to interpret the results obtained.

The scraping of the heat exchanger inner walls eliminates the thermal resistance created by solid PCM and has shown a great performance enhancement with respect to the passive system. During the discharging process, the heat release rate in the SM is kept almost constant and is between two and three times higher than in the nSM, regardless of rotational speed. Therefore, the HTF temperature rise in the SM is always higher and with less variations over time than in the nSM.

The visualization of the solidification process over time allows checking the effectiveness of the scraping process, as well as to measure the evolution of the PCM solid layer thickness over time in the nSM and thus quantifying the solid fraction. Furthermore, after 1 h of experiment, only a 10% of the PCM has solidified with no scraping, whereas the SM is able to extract a 100% of the available latent energy.

A performance comparison between the developed SSHE and those by other authors has been done. The heat release density in this work is similar to those reported in the available bibliography, although the scraping mechanism, the size of the prototypes and their energy capacity are different. Regarding the overall heat transfer coefficient, the SSHE developed in this work has a similar performance to those found in the open literature, though they work at a much higher rotational speed.

The developed design of scraped surface heat exchanger has been shown as a very promising technology to increase the efficiency in solar LTES systems. However, further numerical research will be done in the near future, to complement experimental work. This will allow identifying the optimum heat exchanger operational parameters such as rotational speed, and the temperature difference between the HTF and the solidification point of the PCM.

Declaration of competing interest

The authors declare that they have no known competing financial interests or personal relationships that could have appeared to influence the work reported in this paper.

Acknowledgements

The authors gratefully acknowledge to European Regional Development Fund and Ministerio de Ciencia e Innovación - Agencia Estatal de Investigación for the financial support of the project ALTES: “Active Latent Thermal Energy Storage”, Ref. PGC2018-100864-B-C21. We are also grateful to the company Outheway for the technical support in the design and manufacturing of scraper rotative heat exchanger. The present publication was first presented at the 16th Conference on Sustainable Development of Energy, Water and Environment Systems SDEWES conference, Dubrovnik, Croatia, 10–15 October 2021.

Appendix A. Supplementary data

Supplementary data to this article can be found online at https://doi.org/10.1016/j.renene.2022.05.057.

References

[1] REN21, Renewables 2021 Global Status Report, REN21 Secretariat, Paris, 2021 n.d, https://www.ren21.net/.

[2] P.A. Østergaard, N. Duic, Y. Noorollahi, S. Kalogirou, Latest progress in Sustainable Development using renewable energy technology, Renew. Energy 162 (2020) 1554–1562, https://doi.org/10.1016/j.renene.2020.09.124.

[3] IEA, World Energy Outlook 2021, 2021. Paris, https://www.iea.org/reports/world-energy-outlook-2021.

[4] A. Sharma, A. Shukla, C.R. Chen, T.-N. Wu, Development of phase change materials (PCMs) for low temperature energy storage applications, Sustain. Energy Technol. Assessments 7 (2014) 17–21, https://doi.org/10.1016/j.seta.2014.02.009.

[5] M. Mazman, L.F. Cabeza, H. Mehling, M. Nogues, H. Evliya, H.Ö. Paksoy, Utilization of phase change materials in solar domestic hot water systems, Renew. Energy 34 (2009) 1639–1643, https://doi.org/10.1016/j.renene.2008.10.016.

[6] M.Y. Abdelsalam, H.M. Teamah, M.F. Lightstone, J.S. Cotton, Hybrid thermal energy storage with phase change materials for solar domestic hot water applications: direct versus indirect heat exchange systems, Renew. Energy 147 (2020) 77–88, https://doi.org/10.1016/j.renene.2019.08.121.

[7] G. Alva, Y. Lin, G. Fang, An overview of thermal energy storage systems, Energy 144 (2018) 341–378, https://doi.org/10.1016/j.energy.2017.12.037.

[8] J. Tombrink, H. Jockenhöfer, D. Bauer, Experimental investigation of a rotating drum heat exchanger for latent heat storage, Appl. Therm. Eng. 183 (2021), https://doi.org/10.1016/j.applthermaleng.2020.116221.

[9] M. Fadl, D. Mahon, P.C. Eames, Thermal performance analysis of compact thermal energy storage unit-An experimental study, Int. J. Heat Mass Tran. 173 (2021), 121262, https://doi.org/10.1016/j.ijheatmasstransfer.2021.121262.

[10] N.I. Ibrahim, F.A. Al-Sulaiman, S. Rahman, B.S. Yilbas, A.Z. Sahin, Heat transfer enhancement of phase change materials for thermal energy storage applications: a critical review, Renew. Sustain. Energy Rev. 74 (2017) 26–50, https://doi.org/10.1016/j.rser.2017.01.169.

[11] M. Al-Maghalseh, K. Mahkamov, Methods of heat transfer intensification in PCM thermal storage systems: review paper, Renew. Sustain. Energy Rev. 92 (2018) 62–94, https://doi.org/10.1016/j.rser.2018.04.064.

[12] U. Stritih, An experimental study of enhanced heat transfer in rectangular PCM thermal storage, Int. J. Heat Mass Tran. 47 (2004) 2841–2847, https://doi.org/10.1016/j.ijheatmasstransfer.2004.02.001.

[13] M. Rahimi, A.A. Ranjbar, D.D. Ganji, K. Sedighi, M.J. Hosseini, Experimental investigation of phase change inside a finned-tube heat exchanger, J. Eng. 2014 (2014), 641954, https://doi.org/10.1155/2014/641954.

[14] M. Bortolotti, European Energy Storage Technology Development Roadmap towards 2030 2017 Update, 2017. Brussels, Belgium.

[15] N.H.S. Tay, F. Bruno, M. Belusko, Experimental investigation of dynamic melting in a tube-in-tank PCM system, Appl. Energy 104 (2013) 137–148, https://doi.org/10.1016/j.apenergy.2012.11.035.

[16] J. Gasia, N.H.S. Tay, M. Belusko, L.F. Cabeza, F. Bruno, Experimental investigation of the effect of dynamic melting in a cylindrical shell-and-tube heat exchanger using water as PCM, Appl. Energy 185 (2017) 136–145, https://doi.org/10.1016/j.apenergy.2016.10.042.

[17] S. Zhang, J. Niu, Two performance indices of TES apparatus: comparison of MPCM slurry vs. stratified water storage tank, Energy Build. 127 (2016) 512–520, https://doi.org/10.1016/j.enbuild.2016.05.085.

[18] M. Delgado, A. Lázaro, J. Mazo, C. Peñalosa, J.M. Marín, B. Zalba, Experimental analysis of a coiled stirred tank containing a low cost PCM emulsion as a thermal energy storage system, Energy 138 (2017) 590–601, https://doi.org/10.1016/j.energy.2017.07.044.

[19] V. Zipf, A. Neuhäuser, D. Willert, P. Nitz, S. Gschwander, W. Platzer, High temperature latent heat storage with a screw heat exchanger: design of prototype, Appl. Energy 109 (2013) 462–469, https://doi.org/10.1016/j.apenergy.2012.11.044.

[20] H. Pointner, W.-D. Steinmann, Experimental demonstration of an active latent heat storage concept, Appl. Energy 168 (2016) 661–671, https://doi.org/10.1016/j.apenergy.2016.01.113.

[21] C.A. Acosta, A. Bhalla, R. Guo, Empirical and numerical determination of the freezing point depression of an unsteady flow in a scraped surface crystallizer, Appl. Therm. Eng. 179 (2020), 115734, https://doi.org/10.1016/j.applthermaleng.2020.115734.

[22] M. Ben Lakhdar, R. Cerecero, G. Alvarez, J. Guilpart, D. Flick, A. Lallemand, Heat transfer with freezing in a scraped surface heat exchanger, Appl. Therm. Eng. 25 (2005) 45–60, https://doi.org/10.1016/j.applthermaleng.2004.05.007.

[23] D.S. Martínez, J.P. Solano, P.G. Vicente, A. Viedma, Flow pattern analysis in a rotating scraped surface plate heat exchanger, Appl. Therm. Eng. 160 (2019), 113795, https://doi.org/10.1016/j.applthermaleng.2019.113795.

[24] J.P. Solano, A. García, P.G. Vicente, A. Viedma, Flow pattern assessment in tubes of reciprocating scraped surface heat exchangers, Int. J. Therm. Sci. 50 (2011) 803–815, https://doi.org/10.1016/j.ijthermalsci.2010.11.019.

[25] U. Nepustil, D. Laing-Nepustil, D. Lodemann, R. Sivabalan, V. Hausmann, High temperature latent heat storage with direct electrical charging – second generation design, Energy Proc. 99 (2016) 314–320, https://doi.org/10.1016/j.egypro.2016.10.121.

[26] N. Maruoka, T. Tsutsumi, A. Ito, M. Hayasaka, H. Nogami, Heat release characteristics of a latent heat storage heat exchanger by scraping the solidified phase change material layer, Energy 205 (2020), 118055, https://doi.org/10.1016/j.energy.2020.118055.

[27] J. Tombrink, D. Bauer, Simulation of a rotating drum heat exchanger for latent heat storage using a quasistationary analytical approach and a numerical transient finite difference scheme, Appl. Therm. Eng. 194 (2021), 117029, https://doi.org/10.1016/j.applthermaleng.2021.117029.

[28] M. Kenisarin, K. Mahkamov, Solar energy storage using phase change materials, Renew. Sustain. Energy Rev. 11 (2007) 1913–1965, https://doi.org/10.1016/j.rser.2006.05.005.

[29] A.K. Pandey, M.S. Hossain, V.V. Tyagi, N. Abd Rahim, J.A.L. Selvaraj, A. Sari, Novel approaches and recent developments on potential applications of phase change materials in solar energy, Renew. Sustain. Energy Rev. 82 (2018) 281–323, https://doi.org/10.1016/j.rser.2017.09.043.

[30] Rubitherm GmbH. https://www.rubitherm.eu/, 2014.

[31] S.J. Kline, F.A. McClintock, Describing uncertainty in single sample experiments, Mech. Eng. 75 (1953) 3–8.